Generalized SCIDAR measurements at San Pedro Mártir. II. Wind profile statistics

R. Avila, E. Carrasco, F. Ibañez, J. Vernin, J.-l. Prieur, D. X. Cruz

Generalized SCIDAR Measurements at San Pedro Mártir. II. Wind Profile Statistics

R. Avila[1]

Centro de Radioastronomía y Astrofísica, Universidad Nacional Autónoma de México, Apartado Postal 3-72, Morelia, Michoacán, C. P. 58089, México, r.avila@astrosmo.unam.mx

E. Carrasco

Instituto Nacional de Astrofísica, Óptica, y Electrónica, Luis Enrique Erro 1, Tonantzintla, Puebla, C. P. 72840, México, bec@inaoep.mx

F. Ibañez

Centro de Radioastronomía y Astrofísica, Universidad Nacional Autónoma de México, Apartado Postal 3-72, Morelia, Michoacán, C. P. 58089, México

J. Vernin

Laboratoire Universitaire d'Astrophysique de Nice (UMR 6525), Université de Nice Sophia Antipolis, Parc Valrose, 06108 Nice Cedex 2, France; Jean.VERNIN@unice.fr

J.-L. Prieur

Laboratoire Universitaire d'Astrophysique (UMR 5572), Observatoire Midi-Pyrénées, CNRS, 14 Avenue Edouard Belin, 31400 Toulouse, France; prieur@ast.obs-mip.fr

and

D. X. Cruz

Instituto de Astronomía, Universidad Nacional Autónoma de México, Apartado Postal 70-264, Ciudad de México, D. F., C. P. 04510, México; xochitl@astroscu.unam.mx

ABSTRACT. We present the results of monitoring the speed of optical turbulent layers in the atmosphere above San Pedro Mártir, Mexico, during 15 nights in 2000 May. The data were obtained using the generalized scintillation detection and ranging technique (generalized SCIDAR), developed at Nice University. This paper constitutes the second in a series. The first paper presents results concerning measurements of optical turbulence strength obtained at the same site and time. The principal results of the present article are as follows: (1) The wind profiles remain stable during each night. (2) No correlation between the turbulence intensity C_N^2 and the speed of the turbulent layers, V, is detected for speeds lower than ~45 m s^{-1}. Above that speed, which was only exceeded in the jet-stream layer on one night, the optical turbulence strength is seen to increase. (3) Layers in the first 4 km and higher than 16 km above sea level are similarly slow, with median speeds of 8.6 and 9.6 m s^{-1}, respectively. (4) Between 9 and 16 km, where the jet stream flows on some of the nights, the median wind speed is 26.0 m s^{-1}. (5) From simultaneous measurements of $C_N^2(h)$ and $V(h)$, we compute the temporal coherence of the turbulence, layer by layer, in 500 m thick layers. This is the first time that such data have been published. For a multiconjugate adaptive optics system, our measurements show that the temporal responses of three deformable mirrors conjugated on the ground and at 6 km and 13 km above sea level, each one correcting for the turbulence in 500 m thick layers, would need to be 64, 40, and 20 ms. (6) The vertical variation of V dominates the vertical variation of the coherence time. (7) For the first time, we compare wind velocity profiles obtained from three different sources: generalized SCIDAR, NCEP/NCAR (National Centers for Environmental Prediction/National Center for Atmospheric Research) reanalysis data, and meteorological research balloons. The comparison shows excellent agreement in both the modulus and the direction of the wind velocity.

1. INTRODUCTION

Optical turbulence layers in the Earth's atmosphere are responsible for the deformation of the incoming wave fronts in astronomical observations, which in turn degrade angular resolution. Adaptive optical systems are aimed at full or partial recovery of the limited angular resolution of the telescope. Current development of such systems for existing or future telescopes involves several deformable mirrors, each optically conjugated at different altitudes. These systems are known as multiconjugate adaptive optics (MCAO). Of particular impor-

[1] Work partially done at the Instituto de Astronomía, UNAM, México, D.F., México.

tance is the application of MCAO for extremely large telescopes. The proper development of MCAO systems requires increasingly detailed studies of the optical turbulence in the atmosphere. Apart from the turbulence outer scale and its effects, all the relevant parameters for the characterization of optical turbulence, in the context of astronomical observations, can be derived from the vertical profile of the refractive index structure constant $C_N^2(h)$ (commonly referred to as the turbulence profile) and the vertical profile of the turbulence-layer velocity $\boldsymbol{V}(h)$,[2] where h denotes altitude. For example, the Fried parameter r_0 and the isoplanatic angle θ_0 can be calculated from the integral of $C_N^2(h)$ with respect to h and the 5/3-order moment of h weighed by $C_N^2(h)$, respectively, while the wave-front coherence time τ_0 is obtained from r_0 and the 5/3-order moment of $V(h)$ weighed by $C_N^2(h)$ (Vernin & Muñoz-Tuñón 1994), where V denotes the modulus of $\boldsymbol{V}$. These are examples of parameters that refer to the wave front located at the entrance pupil of the telescope. The development of MCAO also requires knowledge of the altitude and turbulence intensity of the predominant turbulence layers and their displacement velocity in order to determine the spatial and temporal requirements [retrieved from $C_N^2(h)$ and $\boldsymbol{V}(h)$] of each of the wave-front sensors and deformable mirrors in the system. Using predicting filters, such as a Kalman-type filter, it is possible to configure the mirrors of a MCAO system for a given time by (1) taking into account the corrections performed in the past and (2) using information about the modulus and direction of the turbulent-layer velocity. It would then be possible to anticipate most of the correction to be performed for a given time. This would improve the performance of a MCAO system and decrease its response time. Hence, wind speed and wind direction are two key parameters for operating future MCAO systems. Moreover, the selection of the sites where the next-generation, ground-based telescopes are to be installed requires statistical studies of the C_N^2 and $\boldsymbol{V}$ profiles at those sites.

In this paper we present the results of monitoring $\boldsymbol{V}(h)$ at San Pedro Mártir, Baja California, Mexico, using generalized SCIDAR (generalized scintillation detection and ranging). The instrument provides simultaneous measurements of $\boldsymbol{V}(h)$ and $C_N^2(h)$. Results concerning the turbulence profiles have been presented in Avila et al. (2004, hereafter Paper I). Paper I describes some generalities about the instrument and the measurement campaign. For completeness, in § 2.1 we give the relevant information about the measurement technique and, in § 2.2, a log of the observing campaign. The results are grouped in § 3. Section 3.1 gives a data overview. In § 3.2 we present the statistics of the layer velocities in several slabs of the atmosphere. A study of the vertical profile of the coherence time is given in § 3.3. A comparison of our measurements with wind profiles obtained using research balloons is shown in § 3.4. In that section we also compare our results with wind velocity profiles obtained at different elevations from a global circulation model of NOAA (the National Oceanic and Atmospheric Administration). Finally, § 4 gives a summary and conclusions.

[2] Throughout this paper, symbols in boldface denote two-dimensional vectors, and the same symbols in lightface correspond to the modulus of such vectors.

2. MEASUREMENTS OF *V*-PROFILES

2.1. The GS Method

The method used to measure the velocity of the turbulent layers with the generalized SCIDAR (GS) technique has been extensively explained by Avila et al. (2001) and Prieur et al. (2004). We give here a very succinct summary.

The GS concept consists of taking very short exposure images of the scintillation produced by a double star on a virtual plane located at a distance $h_{\rm GS}$, on the order of a few kilometers, below the pupil plane ($h_{\rm GS} < 0$). The C_N^2 profile can be derived from the mean autocorrelation of those images, whereas wind velocity profiles $\boldsymbol{V}(h)$ can be computed from the mean cross-correlation of images taken at times separated by a constant delay Δt. Note that the mean autocorrelation and mean cross-correlation need to be normalized by the autocorrelation of the mean image. Hereafter, we refer to this mean-normalized cross-correlation simply as cross-correlation.

The method is based on the following principle: We assume that the turbulent structures are carried by the mean wind, without deformation. This assumption is known as the Taylor hypothesis and is valid for short time intervals. In this case, the scintillation pattern produced by a layer at altitude h, where the mean horizontal wind velocity is $\boldsymbol{V}(h)$, moves on the analysis plane a distance of $\boldsymbol{V}(h)\Delta t$ in a time Δt. If the source is a single star, the cross-correlation of images separated by a lapse of Δt would produce a correlation peak located at the point $\boldsymbol{r} = \boldsymbol{V}(h)\Delta t$ on the correlation map. By determining this position, one can deduce $\boldsymbol{V}(h)$ for that layer. As we use a double star, the contribution of the layer at altitude h in the cross-correlation consists of three correlation peaks, which we call a triplet: a central peak located at $\boldsymbol{r} = \boldsymbol{V}(h)\Delta t$ and two lateral peaks separated from the central one by $\pm\boldsymbol{\rho}H$, where H is the distance from the analysis plane to the given layer ($H = h - h_{\rm GS}$) and $\boldsymbol{\rho}$ is the angular separation of the double star. The cross-correlation can be written as

$$C_c^{**}(\boldsymbol{r}, \Delta t) = \int_0^\infty dh\, C_N^2(h) \Big(a\mathcal{C}_c[\boldsymbol{r} - \boldsymbol{V}(h)\Delta t, H] + b\big\{\mathcal{C}_c[\boldsymbol{r} - \boldsymbol{V}(h)\Delta t - \boldsymbol{\rho}H, H] + \mathcal{C}_c[\boldsymbol{r} - \boldsymbol{V}(h)\Delta t + \boldsymbol{\rho}H, H]\big\}\Big), \quad (1)$$

where $\mathcal{C}_c$ is the theoretical cross-correlation of the scintillation produced by a layer at an altitude h and unit C_N^2. It differs from the theoretical autocorrelation $\mathcal{C}$ (Prieur et al. 2004) only by an eventual temporal decorrelation of the scintillation (partial failure of the Taylor hypothesis) and an eventual fluctuation of $\boldsymbol{V}(h)$ during the integration time. The decorrelation would make $\mathcal{C}_c$ smaller than $\mathcal{C}$, and the fluctuation of $\boldsymbol{V}(h)$ would make $\mathcal{C}_c$

TABLE 1
VELOCITY RESOLUTION

Δt (ms)	ΔV (m s^{-1})	
	SPM1.5	SPM2.1
20	1.55	2.05
40	0.77	1.02

smaller and wider than $\mathcal{C}$ (Caccia et al. 1987). Those effects do not affect the determination of $\boldsymbol{V}(h)$, as the only information needed here is the position of each correlation peak. Note that $\mathcal{C}$ takes into account the spatial filtering introduced by the detector sampling. The factors a and b are given by the magnitude difference of the two stars Δm through

$$a = \frac{1+\alpha^2}{(1+\alpha)^2}, \quad b = \frac{\alpha}{(1+\alpha)^2}, \tag{2}$$

with $\alpha = 10^{-0.4\Delta m}$.

2.2. Observing Campaign

The data used in this work were obtained in 2000 May at the Observatorio Astronómico Nacional de San Pedro Mártir (OAN-SPM), Mexico, located at an altitude of 2850 m above sea level. We used the GS system from the Laboratoire Universitaire d'Astrophysique de Nice, France. The instrument was installed on the 1.5 and 2.1 m telescopes (hereafter SPM1.5 and SPM2.1) over nine and seven nights (May 7–15 and 16–22 UT), respectively.

2.3. Instrumental Parameters

The concept of the GS method can be found in a number of papers (Rocca et al. 1974; Avila et al. 1997, 2001; Fuchs et al. 1998; Klückers et al. 1998; Prieur et al. 2001, 2004). In Paper I, the instrumental characteristics concerning the determination of $C_N^2(h)$ were presented. Here we describe the relevant parameters for the determination of $\boldsymbol{V}(h)$.

The scintillation images used for the computation of the cross-correlations are the same as those used for the autocorrelations (see Paper I). The image plane is situated 3 or 4 km below the pupil plane. Images are recorded inside a 64 × 64 window of an intensified CCD. Each pixel covers a square area on the image plane, which has a side Δx equal to 3.1 and 4.1 cm for SPM1.5 and SPM2.1, respectively. The spatial filtering introduced by such pixel sizes is taken into account in the inversion process by convolving the theoretical autocorrelation by the autocorrelation of the impulse response of the camera. The exposure time of each image is 1 or 2 ms, depending on the star's magnitude and the prevailing observing conditions. One image is obtained every 20 ms. The wavelength is centered at 0.5 μm. Two 128 × 128 cross-correlation maps—one for a time lapse of $\Delta t = 20$ ms and another one for $\Delta t = 40$ ms—are saved on disk at time intervals that depend on the number of images used to compute the cross-correlations. Most of the time, this number was equal to 2000, which gives a mean time lag of 1.32 minutes between each registration. The computation of the correlations are performed in quasi–real time, so that only the correlations—and not the images—are stored on disk. Table 1 of Paper I lists the double stars used as light sources.

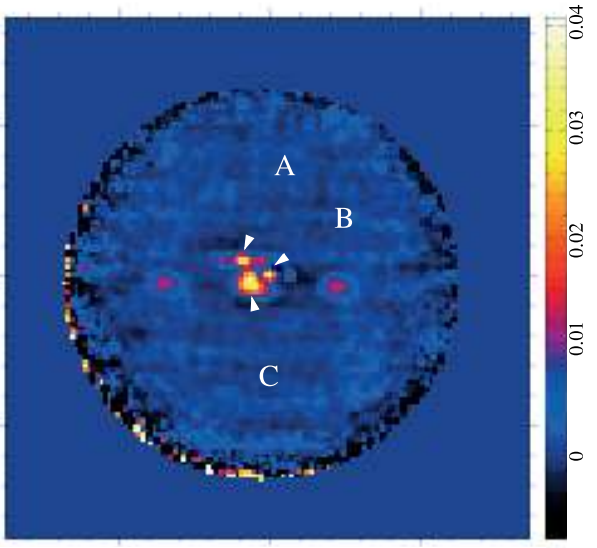

FIG. 1.—Example of a mean cross-correlation. The data were obtained with 2000 scintillation images of the 6.″4 separation double star ζ CrB, with a lag of $\Delta t = 20$ ms between correlated images and the analysis plane conjugated at $h_{GS} = -4$ km. The observation was performed on 2000 May 9, 08:29 UT, at SPM1.5. Three horizontally aligned correlation triplets can be seen (labeled A, B, and C), each corresponding to a turbulent layer. The arrows point to the triplet centers. The color scale indicates normalized cross-correlation values.

Masciadri et al. (2002) presented an analysis of the C_N^2 detectivity level for the same data used here. In their Figure 12, it can be seen that $\Delta C_N^2 \Delta h < 10^{-15}$ m$^{-1/3}$ for SPM2.1 and any of the stars used. Considering that the C_N^2 profiles were resampled to an altitude resolution of $\Delta h = 500$ m, we have $\Delta C_N^2 < 2 \times 10^{-18}$ m$^{-2/3}$ for SPM2.1. From equation (1) of Masciadri et al. (2002), the C_N^2 uncertainty is inversely proportional to the telescope diameter. Hence, for SPM1.5, $\Delta C_N^2 < 2.7 \times 10^{-18}$ m$^{-2/3}$.

The resolution $\Delta \boldsymbol{V}$ of the wind velocity determination is set by $\Delta \boldsymbol{V} = (\Delta x \sec z)/\Delta t$, where z is the zenith angle. Table 1 gives the velocity resolution for each telescope for each Δt value, with $z = 0$.

2.4. Data Reduction

The method used to obtain the velocity profiles from the cross-correlation data is based on an interactive algorithm that is extensively explained by Avila et al. (2001). Prieur et al. (2004) presented an automatic version of that algorithm. For

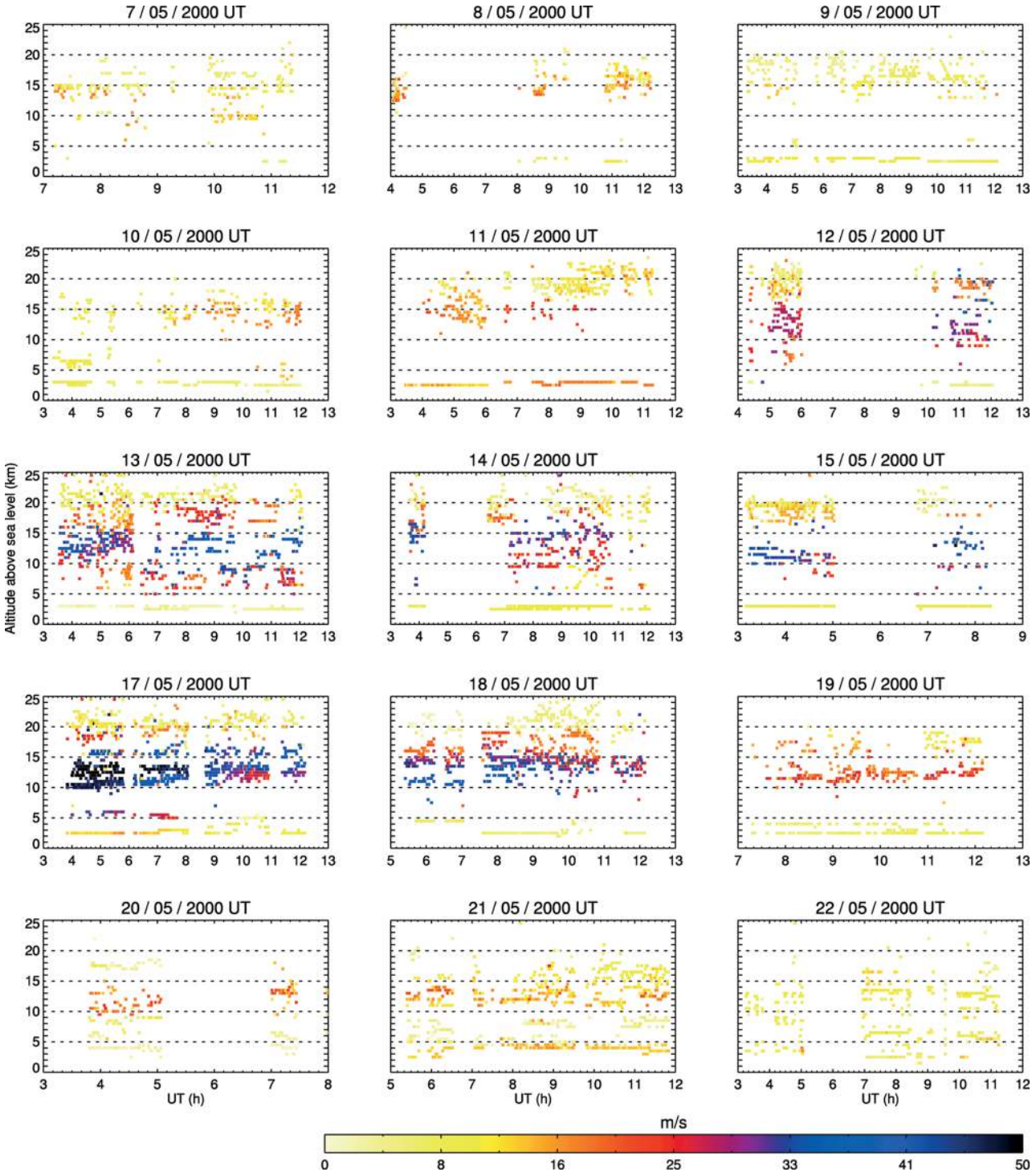

FIG. 2.—Mosaic of the wind profiles measured during the whole campaign. Each panel corresponds to one night. The vertical and horizontal axes represent the altitude above sea level (observatory altitude is 2850 m) and Universal Time, respectively. The wind speed values are coded with the color scale shown at the bottom. The top three rows and bottom two rows contain the profiles obtained at SPM1.5 and SPM2.1, respectively.

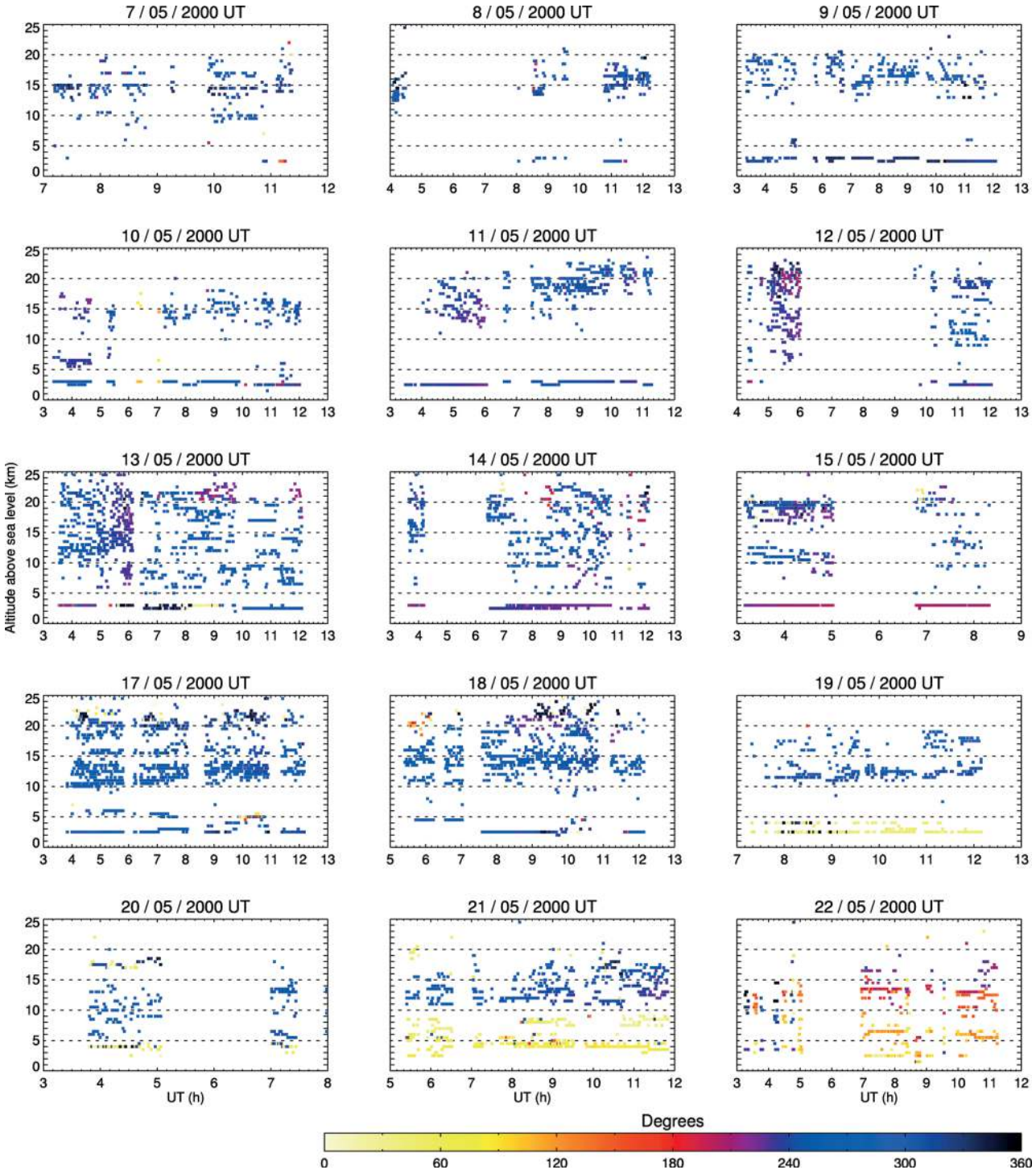

FIG. 3.—Same as Fig. 2, but here the colors represent the direction of the wind, and 0°, 90°, 180°, and 270° correspond to wind blowing from north, east, south, and west, respectively.

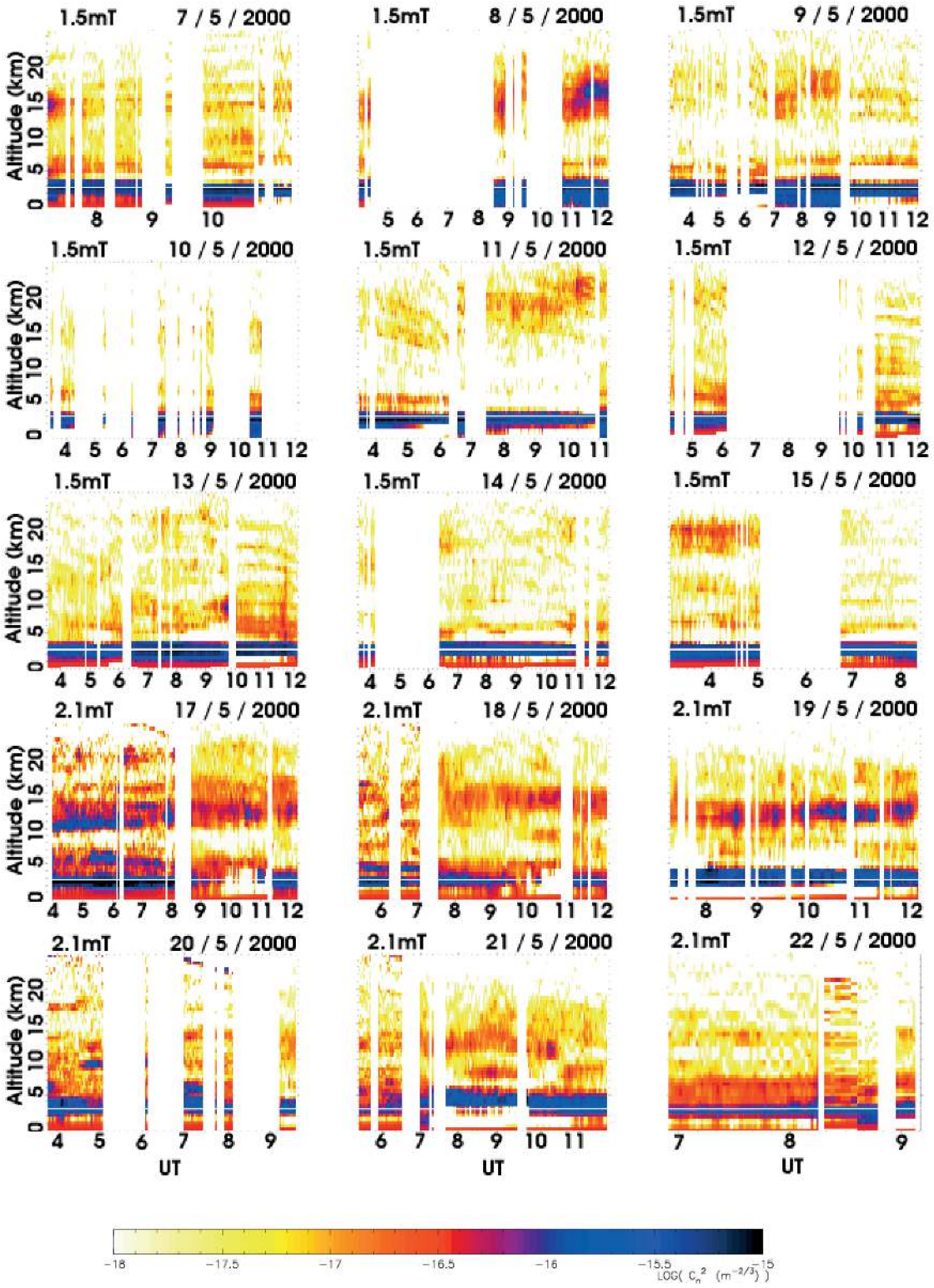

FIG. 4.—Same as Fig. 2, but here the colors represent C_N^2 values coded as shown by the logarithmic scale at the bottom.

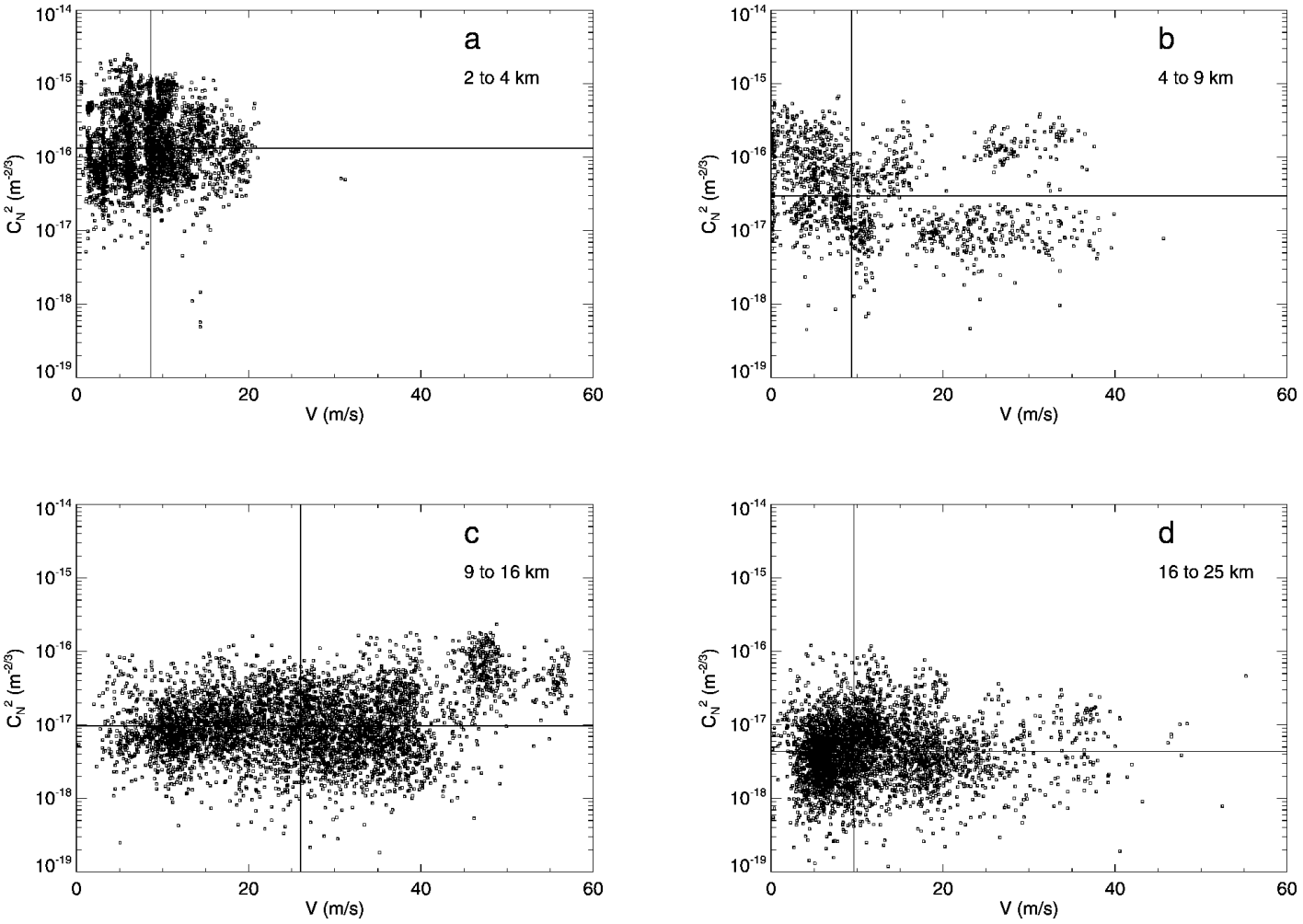

FIG. 5.—C_N^2 plotted vs. V for all the turbulent layers detected. Each panel corresponds to a different altitude range above sea level, as indicated by the labels. The horizontal and vertical lines in each panel indicate the median values of C_N^2 and V, respectively.

the reduction of the data presented here, we have primarily used the interactive algorithm. Part of the data were reduced twice using the automatic algorithm, finding excellent agreement. Here we recall the basis of the interactive algorithm.

Figure 1 shows an example of a cross-correlation map. Three horizontally aligned triplets (labeled A, B, and C) can be seen. As explained in § 2.1, for a given triplet, the distance from the center of the map to the central peak equals $\boldsymbol{V}\Delta t$, which gives $\boldsymbol{V}$, and the distance from the central peak to either of the lateral peaks equals $\boldsymbol{\rho}H$, which gives the layer altitude h through $H = h - h_{\rm GS}$. The interactive algorithm requires the user to point and click on the triplet center and either of the lateral peaks. The program computes the layer velocity $\boldsymbol{V}$ and altitude h and determines the C_N^2 value from the previously obtained $C_N^2(h)$ profile. These data are used to compute a correlation triplet and subtract it from the cross-correlation map.

Sometimes, several layers appear to exist at the same altitude, but with different velocities. Our interpretation is that they are actually situated at slightly different altitudes that cannot be resolved in the C_N^2 profile. In this case, the measured C_N^2 at the altitude of these layers corresponds to the sum of the real C_N^2 of each layer. To determine the individual C_N^2 values, the measured C_N^2 is distributed to the layers at the same altitude using weights that are proportional to the peak amplitudes in each of the corresponding triplets.

The dome seeing is retrieved from the cross-correlation maps. When at least two triplets are detected at the observatory altitude and one of them has a velocity smaller than the velocity resolution, this triplet is interpreted as being generated inside the telescope dome, where the mean wind velocity is zero. The dome seeing is then retrieved, as in the case of multiple layers at apparently the same altitude, as explained above.

3. RESULTS AND DISCUSSIONS

3.1. $V(h)$ Data Overview

We have been able to retrieve 3016 profiles from this observation campaign. Figure 2 shows a mosaic view of all the

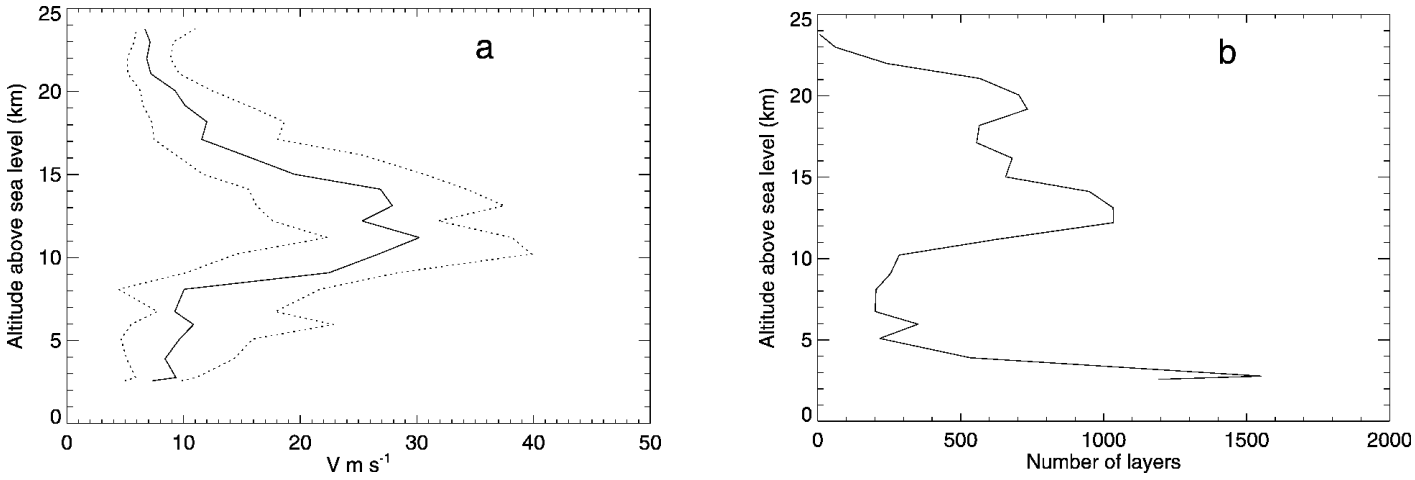

FIG. 6.—(*a*) Profiles of median (*solid line*) and first and third quartiles (*dotted lines*) of the wind speed. (*b*) Profile of the number of data layers used for the statistical calculations. The dome-seeing layer was excluded.

wind speed profiles. It can be seen that at the observatory level, the wind is generally weak. As we have excluded the data corresponding to the dome seeing, wind values at ground level are associated with open-air turbulence.

In many cases, dots with different colors appear superimposed, which indicates the presence of several turbulent layers with altitude differences smaller than the vertical resolution of the C_N^2 profiles, but with detectable velocity differences. This feature constitutes a strong advantage of the simultaneous measurement of $C_N^2(h)$ and $\boldsymbol{V}(h)$, as opposed to the measurement of $C_N^2(h)$ alone. The velocity of the layers represents an additional dimension in the parameter space that characterizes each layer. Therefore, the determination of the velocity of each layer can help to identify individual turbulent layers.

The fastest turbulent layers are found between 9 and 16 km. In this altitude range, a slow modulation of the layer speed from night to night can be noticed: during the first four nights, the speed was lower than 20 m s^{-1}, then it started to increase, reaching 55 m s^{-1} on May 17 UT, and then decreased to values lower than 10 m s^{-1}, and was generally lower than 10 m s^{-1} on the last night.

The wind direction profiles are shown in Figure 3. It can be seen that the wind blows predominantly from west to east (i.e., around 270°) at every altitude. In general, the wind direction varies very little as a function of altitude. However, on May 21 UT, there was a steep variation of the wind direction at approximately 10 km that lasted all night long. The following night, the same gradient in wind direction was still present, but less pronounced.

In Figure 4 we reproduce Figure 1 of Paper I, which represents a mosaic view of the C_N^2 profiles that were obtained using the same data that was used for the wind profiles. From a visual inspection of Figures 2 and 4, it can be seen that only on the night of May 17 UT and in the jet-stream layer is there an evident correlation between C_N^2 and wind speed values. To confirm this, Figure 5 plots the C_N^2 values against the layer speeds for all the layers detected in the campaign. Panels correspond to different altitude intervals. No correlation between V and C_N^2 is detectable for speeds lower than ∼45 m s^{-1}. Above that speed, which was only exceeded in the jet-stream layer on May 17 UT, the optical turbulence strength is seen to increase. The general lack of correlation seen between C_N^2 and V might be due to the fact that local optical turbulence is triggered by *vertical* instabilities induced by shears on scales that are generally much smaller than the 500 m altitude resolution of the C_N^2 profiles obtained using GS. The detected optical turbulence is therefore diluted by the averaging process. In a high-speed jet stream, wind shear most likely prevails almost everywhere, resulting in an enhanced median C_N^2. In any case, optical turbulence strength also depends on the vertical gradient of the potential temperature. This additional independent parameter contributes to the lack of correlation between V and C_N^2. Coulman et al. (1995) studied in detail the relation between C_N^2, velocity gradient, and potential temperature gradient using meteorological balloon measurements. It would be interesting to perform a similar study and enrich it by adding a comparison with GS data obtained at the same time as the balloon data. Such a study is beyond the scope of the present paper.

3.2. Wind Speed Profile Statistics

Using all the measured $\boldsymbol{V}$-profiles, we have computed the median and first and third quartile values of the layer speed V as a function of height. The corresponding plots are shown in Figure 6*a*. It can be seen that the wind speed has low values that are similar near the ground (within the first 4 km) and above 16 km. In the jet-stream zone, the wind speed sharply increases. The significance of the statistical values for each altitude is indicated by the number of measurements used in

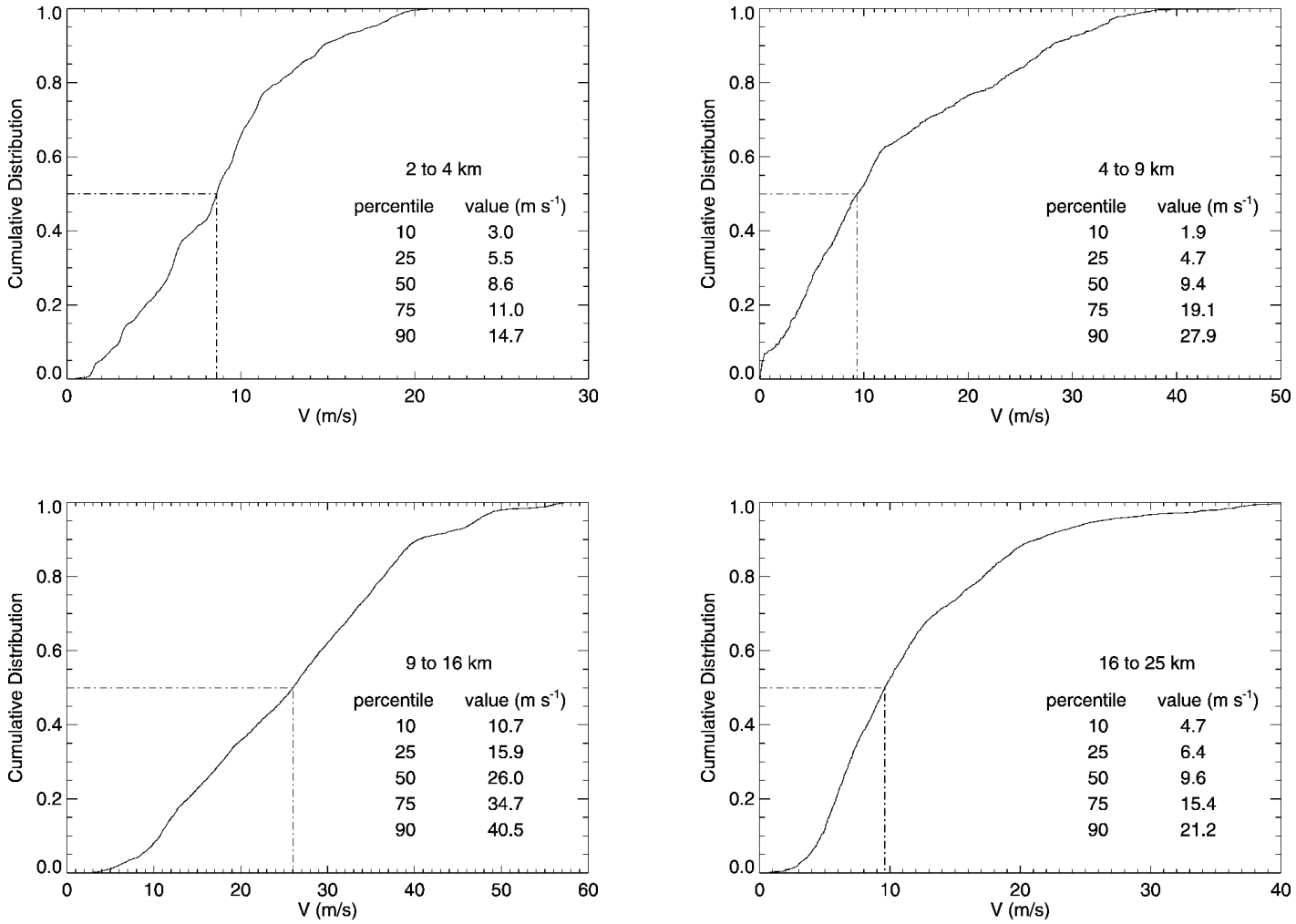

FIG. 7.—Cumulative distribution of the wind values in the altitude ranges indicated in each panel. The dome-seeing layer was excluded for the 2–4 km altitude range.

the computation (i.e., the number of detected layers shown in Fig. 6*b*).

A more complete statistical description of the wind speed values is obtained from their cumulative distribution function (CDF), which corresponds, for each value of V, to the probability of occurrence of such a value or a lower one. We computed one CDF for the wind values grouped in each of four altitude intervals: 2–4, 4–9, 9–16, and 16–25 km above sea level, as shown in Figure 7. We can see, for example, that 10% of the V-values are lower than 3.0, 1.9, 10.7, and 4.7 m s^{-1} in the 2–4, 4–9, 9–16, and 16–25 km slabs, respectively, and 10% of the values are higher than 14.7, 27.9, 40.5, and 21.2 m s^{-1}. These numbers characterize the extreme wind conditions at each altitude interval.

3.3. Coherence Time Profiles

From the C_N^2 and V values of each detected layer, the coherence time τ of the wave-front deformations produced by that layer can be calculated using an expression that is analogous to that given by Roddier (1999):

$$\tau = 0.31(r_{0_{\rm ind}}/V), \tag{3}$$

where $r_{0_{\rm ind}}$ corresponds to the Fried parameter that would occur if only the given layer was present:

$$r_{0_{\rm ind}} = [0.423\,(2\pi/\lambda)^2\,C_{N\Delta h}^2]^{-3/5}\,, \tag{4}$$

where the wavelength $\lambda = 0.5$ μm. The value of τ for a given layer is defined such that if the time delay of a deformable mirror conjugated to that layer is less than τ, then the mean square phase error that is due only to the time delay will be smaller than 1 rad. We have calculated $\tau(h)$ from each C_N^2 and V profile, taking Δh to be 500 m (i.e., equal to our C_N^2 profile sampling). The median and first and third quartiles of $\tau(h)$ are shown in Figure 8. From the median C_N^2 profile measured at

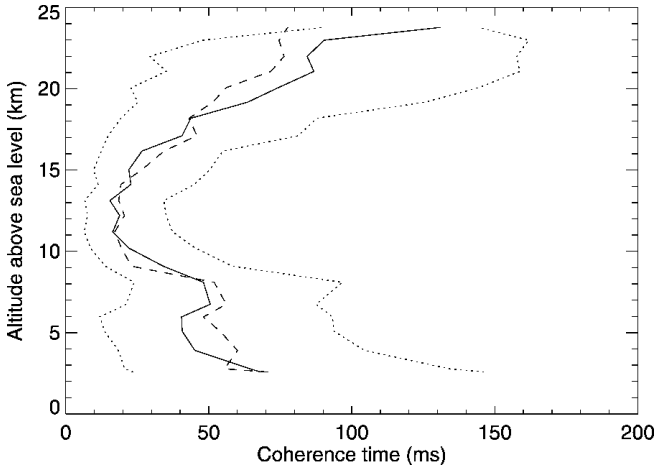

FIG. 8.—Median (*solid line*) and first and third quartile profiles (*dotted lines*) of the coherence time for adaptive optics, as explained in the text (eqs. [3] and [4]). The dashed line represents the coherence time profile computed using eq. (5).

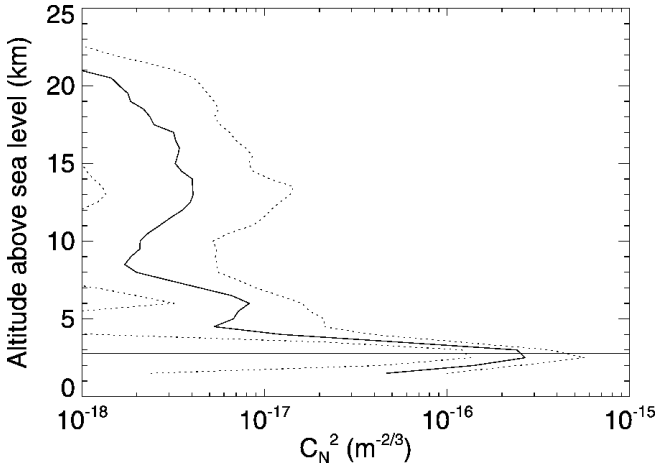

FIG. 9.—Median (*solid line*) and first and third quartiles (*dashed lines*) of the $C_N^2(h)$ values obtained with GS at SPM on both telescopes. The horizontal axis represents C_N^2 values on a logarithmic scale, and the vertical axis represents the altitude above sea level. The horizontal line indicates the observatory altitude. Dome seeing has been removed.

SPM in 2000 (shown in Fig. 9), one could envisage a MCAO system consisting of three deformable mirrors conjugated at ground level and 6 and 13 km above sea level. For such conjugation altitudes, the median value of τ would be approximately 64, 40, and 20 ms, respectively.

It is interesting to note that the variation of τ with altitude seems to be mainly governed by the variation of V. This is shown by the reasonably good agreement between the median of $\tau(h)$ and the median of the function

$$\tau_*(h) = 0.31[r_{0_{\rm med}}/V(h)], \tag{5}$$

where $r_{0_{\rm med}} = 1.8$ m is the median value of $r_{0_{\rm ind}}$ for all altitudes and all turbulence profiles (we remind the reader that $r_{0_{\rm ind}}$ is computed for 500 m slabs). The median profiles of $\tau(h)$ and $\tau_*(h)$ are shown as solid and dashed lines, respectively, in Figure 8. The strong dependence of the variation of τ with height on that of V can be explained by the analysis of the derivative of equation (3):

$$\Delta\tau = 0.31\,\frac{\Delta r_{0_{\rm ind}}\bar{V} - \bar{r}_{0_{\rm ind}}\Delta V}{\bar{V}^2}. \tag{6}$$

The pertinent comparison here is between the terms $\Delta r_{0_{\rm ind}}\bar{V}$ and $\bar{r}_{0_{\rm ind}}\Delta V$. Taking $\bar{V}$ and $\bar{r}_{0_{\rm ind}}$ as the median values of V and $r_{0_{\rm ind}}$, and ΔV and $\Delta r_{0_{\rm ind}}$ as the variation of the corresponding parameters with height—that is, the standard deviation of the values of the median profiles of V and $r_{0_{\rm ind}}$—we obtain $\bar{V} = 10.1$ m s^{-1}, $\bar{r}_{0_{\rm ind}} = 1.8$ m, $\Delta V = 8.1$ m s^{-1}, and $\Delta r_{0_{\rm ind}} = 0.4$ m. Thus, $\Delta r_{0_{\rm ind}}\bar{V} = 4.04$ and $\bar{r}_{0_{\rm ind}}\Delta V = 14.58$, which indicates that ΔV has almost 4 times more impact on $\Delta\tau$ than $\Delta r_{0_{\rm ind}}$.

This is the first time that a study of τ-profiles has been published. It is extremely useful for the development of the next generation of adaptive optics systems.

3.4. Comparison with Other Measurements and Data Sets

The goal of this section is to compare three different values of the wind velocity profiles: those obtained with the GS system, the wind speed measured simultaneously from balloons, and values for the same nights obtained from the global circulation model NCEP/NCAR (National Centers for Environmental Prediction/National Center for Atmospheric Research) Reanalysis Project. This is the first published comparison between GS and NCEP/NCAR wind profiles.

The balloons that were used are described by Azouit & Vernin (2005). The wind values are retrieved from the temporal derivative of the balloon's horizontal position.

The NCEP/NCAR Reanalysis Project database model uses a state-of-the-art analysis and forecasting system to perform data assimilation using data from 1948 to the present. It is considered to be one of the most reliable fields analyzed (Kisler et al. 2001), as it is constrained by observational information, such as land, marine, balloon, satellite, and aircraft data. The Climate Diagnostics Center–derived NCEP Reanalysis Products include U and V components of wind velocity every 6 hr at 17 different pressure levels.

San Pedro Mártir's geographic coordinates are $+31\overset{\circ}{.}05$ latitude and $-115\overset{\circ}{.}47$ longitude, while the grid points closest to the SPM coordinates are $+30\overset{\circ}{.}00$ and $-115\overset{\circ}{.}0$, respectively. We assume a standard atmosphere in order to associate the 17 pressure levels with altitudes (e.g., 200 mbar corresponds to 12 km above sea level). For each altitude, we obtained the velocity module from the U and V components for the four daily forecasted values.[3] For the purposes of comparisons with

[3] Wind blows to the east and north for $U > 0$ and $V > 0$, respectively.

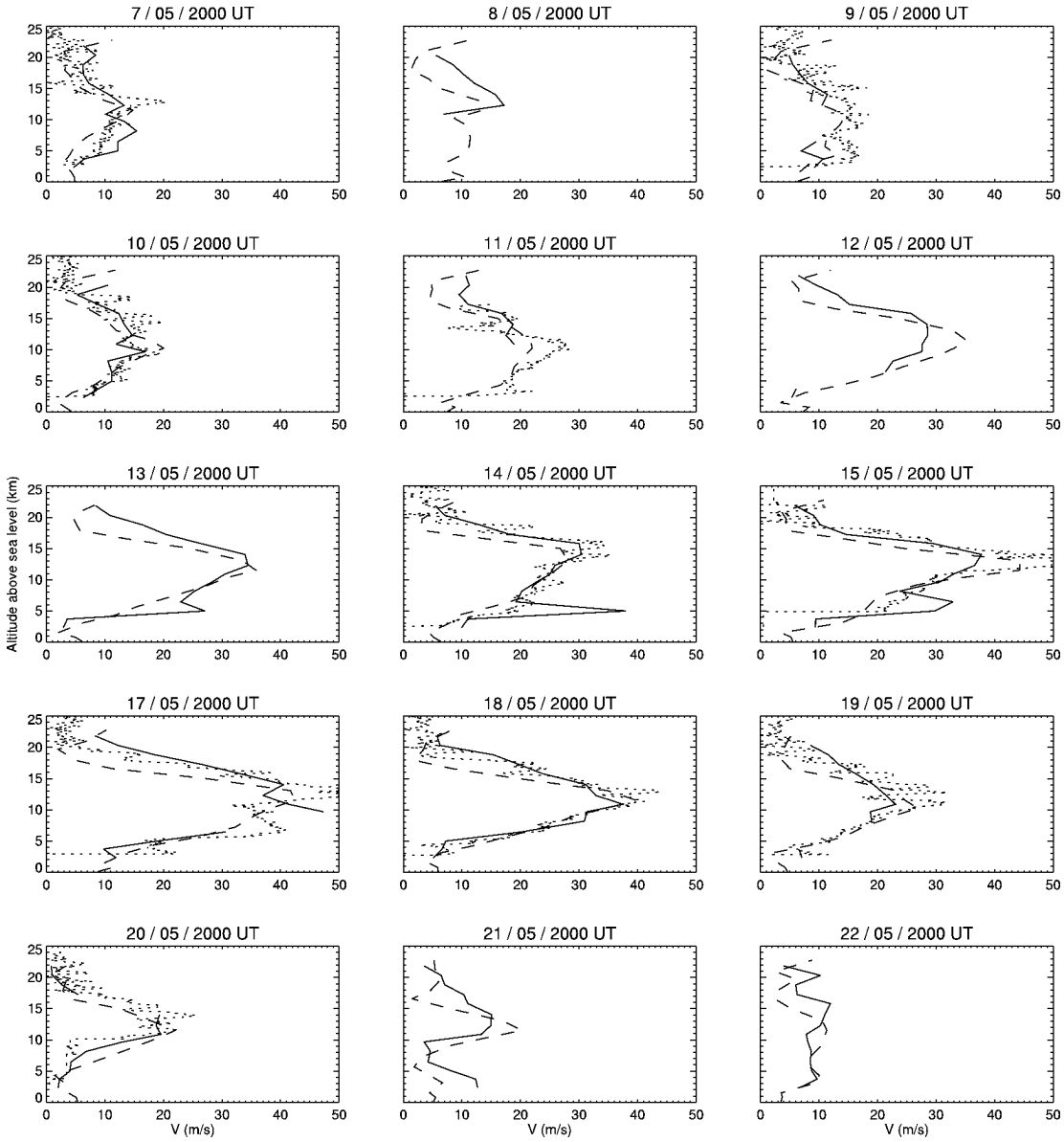

FIG. 10.—Same as Fig. 2, but here each panel shows the mean speed profile as measured with GS (*solid lines*), wind profiles obtained from the NCEP/NCAR Reanalysis Project (*dashed lines*), and wind profiles measured with balloons (*dotted lines*). The GS profiles exclude dome turbulence. The NCEP/NCAR Reanalysis Project profiles are averages of the 06:00 and 12:00 UT data. Each balloon profile corresponds to a single balloon launch. On some nights, there were no balloon data.

GS data, we average only the 06:00 and 12:00 UT wind velocity values.

The comparison of the wind speed profiles for 15 nights are shown in Figure 10, with the date indicated on top of each panel. The solid lines correspond to the mean speed profiles obtained each night using GS, excluding dome turbulence. The dotted lines show the wind speeds measured with balloons, when available. There was at most one balloon flight per night. The wind speed profiles obtained from the NCEP/NCAR reanalysis model are shown as dashed lines. A visual comparison shows very good agreement between the three data sets. The NCEP/NCAR Reanalysis Project profiles reproduce the GS and balloon measurements remarkably well, with the exception of the GS features shown on May 13, 14, and 15 at about 5 km, which are due to isolated intense wind misdetections, as can be seen in Figure 2. The higher resolution of the balloon measurements shows spatial wind speed fluctuations that could not be appreciated otherwise.

The wind direction profiles obtained with the three different methods are plotted in Figure 11. The agreement below 20 km

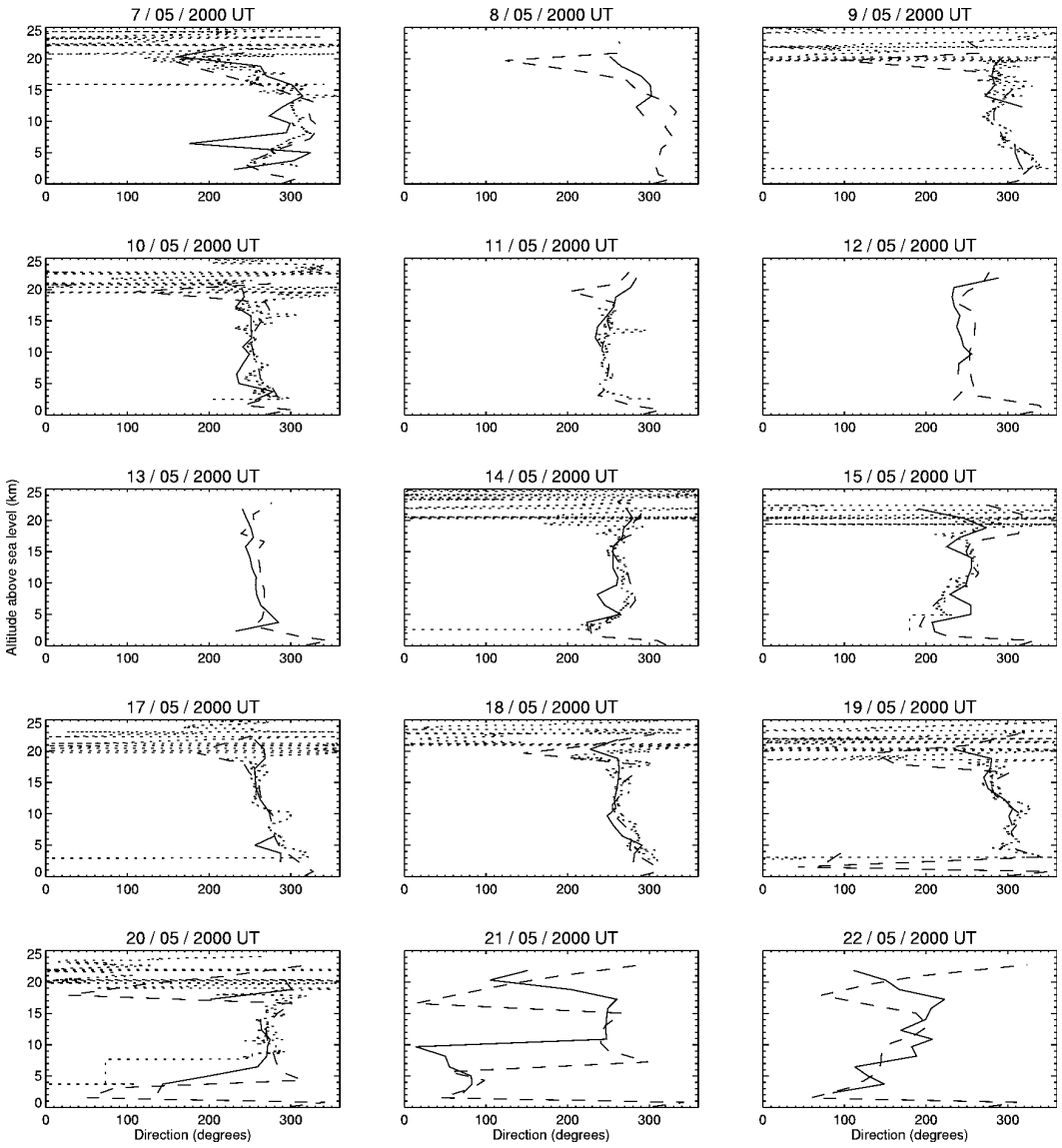

FIG. 11.—Same as Fig. 10, but here each panel shows the wind direction profile as obtained with GS (*solid lines*), the NCEP/NCAR Global Reanalysis Project (*dashed lines*), and those measured with the balloons (*dotted lines*). Wind blowing from the north, east, south, and west correspond to 0°, 90°, 180°, and 270°, respectively. As in Fig. 10, during some nights there were no balloon data.

is generally remarkable. Above that level, the balloons measured winds in virtually any direction. We believe that this is due to the extremely weak wind speed above 20 km.

This cross comparison provides confidence in all three methods for the determination of wind speed profiles. Particularly, it indicates that for prospective site evaluations, it may suffice to determine the wind speed profile from the NCEP/NCAR Reanalysis Project, rather than actually measure the profiles at a given site. The advantage of the GS measurements is that they provide the velocity of the turbulence layers themselves, which is what really matters for high angular resolution techniques.

4. SUMMARY AND CONCLUSIONS

We present the results of measurements of the speed and intensity of optical turbulent layers above the Observatorio Astronómico Nacional de San Pedro Mártir, Mexico, performed using GS during 15 nights in 2000 May. The analysis was performed on a data set from which we could exclude telescope dome turbulence.

The wind profiles remained fairly stable during each night. The wind speed variations occurred on timescales of several nights. A general lack of correlation was found between C_N^2 and V, except in the case where the speed exceeded ~45 m s^{-1}, when

C_N^2 was seen to increase. This condition was met only in the jet-stream layer during one night. The median wind profile shows wind velocities that are similarly low in the slabs that go from the ground up to 4 km and from 16 to 25 km. In between, the wind is much stronger, due to the jet stream.

Using the wind and turbulence profiles, we present the first published computation of layer-oriented temporal coherence, which is particularly useful for the development of multiconjugate adaptive optics systems. This analysis shows that the temporal responses of three hypothetical deformable mirrors conjugated on the ground and at 6 and at 13 km above sea level, each one correcting for the turbulence in 500 m thick layers, would be 64, 40, and 20 ms, respectively. The variation of coherence time with height seems to be governed by a variation of the wind profile with height. Such a study of the coherence time can only be obtained from simultaneous C_N^2 and $\boldsymbol{V}$ profiles.

The results of this paper illustrate the usefulness of wind velocity profile measurements performed with the GS technique. The consistency of those measurements with other means of wind profile determination, namely meteorological balloon measurements and NCEP/NCAR Reanalysis Project data, has been demonstrated. For the evaluation of a virgin site, GS is not a suitable method, as it requires a telescope at least 1 m in diameter. In that case, the NCEP/NCAR Reanalysis Project wind profiles are best suited. It has been shown here that NCEP/NCAR Reanalysis Project data can be appropriate for determining both wind speed and wind direction profiles, with very good precision. If $C_N^2(h)$ models are required, one might employ a simulation code, such as Meso-NH (Masciadri et al. 1999a, 1999b, 2004). Should actual $C_N^2(h)$ and $\boldsymbol{V}(h)$ measurements be needed at a virgin site, one possibility is to use single star SCIDAR, which is being developed at Nice University (Habbib et al. 2005).

We are indebted to the referee, René Racine, whose queries enhanced the presentation of the paper and led to deeper insights on various aspects. The valuable support of the OAN-SPM staff is gratefully acknowledged. This work was done in the framework of a collaboration between the Instituto de Astronomía of the Universidad Nacional Autónoma de México and the UMR 6525 Astrophysique, Université de Nice, Sophia Antipolis (France), supported by ECOS-ANUIES grant M97U01. Funding was also provided by grants J32412E from CONACyT, IN118199 and IN111403 from DGAPA-UNAM, and the TIM project (IA-UNAM). NCEP Reanalysis Project data were provided by the NOAA-CIRES Climate Diagnostics Center, Boulder, Colorado, from their Web site at http://www.cdc.noaa.gov.

REFERENCES

Avila, R., Masciadri, E., Vernin, J., & Sánchez, L. 2004, PASP, 116, 682 (Paper I)
Avila, R., Vernin, J., & Masciadri, E. 1997, Appl. Opt., 36, 7898
Avila, R., Vernin, J., & Sánchez, L. J. 2001, A&A, 369, 364
Azouit, M., & Vernin, J. 2005, PASP, 117, 536
Caccia, J.-L., Azouit, M., & Vernin, J. 1987, Appl. Opt., 26, 1288
Coulman, C. E., Vernin, J., & Fuchs, A. 1995, Appl. Opt., 34, 5461
Fuchs, A., Tallon, M., & Vernin, J. 1998, PASP, 110, 86
Habbib, A., Vernin, J., & Benkhaldoun, Z. 2005, CR Acad. Sci. Paris, 6, 385
Kisler, R., et al. 2001, Bull. Am. Meteor. Soc., 82, 247
Klückers, V. A., Wooder, N. J., Nicholls, T. W., Adcock, M. J., Munro, I., & Dainty, J. C. 1998, A&AS, 130, 141
Masciadri, E., Avila, R., & Sánchez, L. J. 2002, A&A, 382, 378
———. 2004, Rev. Mex. AA, 40, 3
Masciadri, E., Vernin, J., & Bougeault, P. 1999a, A&AS, 203, 137
———. 1999b, A&AS, 137, 185
Prieur, J.-L., Avila, R., Daigne, G., & Vernin, J. 2004, PASP, 116, 778
Prieur, J.-L., Daigne, G., & Avila, R. 2001, A&A, 371, 366
Rocca, A., Roddier, F., & Vernin, J. 1974, J. Opt. Soc. Am. A, 64, 1000
Roddier, F. 1999, Adaptive Optics in Astronomy (Cambridge: Cambridge Univ. Press)
Vernin, J., & Muñoz-Tuñón, C. 1994, A&A, 284, 311